An Anisotropic Material Model for Image Guided Neurosurgery

Corey A. Kemper[1], Ion-Florin Talos[2], Alexandra Golby[2], Peter M. Black[2], Ron Kikinis[2], W. Eric L. Grimson[1], and Simon K. Warfield[2]

[1] Massachusetts Institute of Technology, Cambridge, MA 02139
[2] Departments of Neurosurgery and Radiology, Brigham and Women's Hospital, Harvard Medical School, Boston, MA 02115

Abstract. In order to combine preoperative data with intraoperative scans for image-guided neurosurgery visualization, accurate registration is necessary. It has been determined previously that a suitable way to model the non-rigid deformations due to brain shift is via a biomechanical model that treats the brain as a homogeneous, isotropic, linear elastic solid. This work extends that model-based non-rigid registration algorithm to take into account the underlying white matter structure, derived from diffusion tensor MRI, to more accurately model the brain. Experiments performed on retrospective surgical cases were used to evaluate the results of the registration algorithm in comparison to the earlier model.

1 Introduction

Medical imaging has played an increasingly important role in surgical planning and treatment because it provides valuable information about anatomical structure and function. This has been particularly helpful for neurosurgical procedures, where the surgeon is faced with the challenge of removing as much tumor as possible without damaging the healthy brain tissue surrounding it. Regions important to function are often visually indistinguishable and may have been displaced or even infiltrated by the growth of the tumor. However, an abundance of information is available to the neurosurgeon from data derived from a variety of imaging modalities that can address these difficulties.

The development of image-guided neurosurgery (IGNS) methods over the past decade has permitted major advances in minimally invasive therapy delivery. Visualization of the images acquired during IGNS can be enhanced by preoperatively acquired data, whose acquisition and subsequent processing are not limited by any time restriction. For example, conventional MRI provides high resolution anatomical information with increased spatial resolution and contrast, functional MRI provides maps that are correlated with the activation of specific regions of the brain, MR angiography provides the locations of blood vessels, and diffusion tensor MRI (DT-MRI) provides information on the structure of the white matter.

The first issue in utilizing multimodal preoperative data in conjunction with intraoperative images is to correct for patient motion, which is generally limited

C. Barillot, D.R. Haynor, and P. Hellier (Eds.): MICCAI 2004, LNCS 3217, pp. 267–275, 2004.

to rotation and translation of the skull. However, clinical experience has exposed the limitations of these registration and visualization approaches. During neurosurgical procedures, the brain undergoes non-rigid deformations, and the spatial coordinates of brain structures and adjacent lesions may change significantly.

Most models of deformation either represent the brain as some kind of elastic solid or consolidated material [1,4,6,12]. The most significant limitation at the present time is the computational overhead associated with calculating a Finite Element solution for each update, which limits the complexity of the model that is practical for use in IGNS. Therefore, highly complex models, such as the hyperviscoelastic one described by Miller and Chinzei [7], are not yet appropriate for our application. However, the accuracy of the registration depends on how well the model represents the brain, so we attempt to balance the considerations of accurate modeling and computation time.

The goal of this work was to extend a physics-based biomechanical model for non-rigid registration, designed and developed by Ferrant [2], by incorporating the underlying structure of the brain tissue to better capture changes in the brain shape as it deforms. The deformations estimated by the model were then applied to preoperatively acquired data of different modalities, including fMRI, MRA, and DT-MRI, in order to make the information provided by such data available to the surgeon during the procedure. To meet the real-time constraints of neurosurgery, we utilize a series of scripts [10], which take advantage of high performance computing, to run our registration algorithm.

For validation, the registration algorithm was applied to several surgical cases retrospectively. The registration results were compared to those of the isotropic linear elastic model in order to evaluate the amount, if any, of improvement in registration accuracy was made by extending the model.

2 Method

2.1 Elasticity Model

For the biomechanical model implemented by Ferrant [2] and extended here, the brain is treated as a linear elastic solid. Assuming a linear elastic continuum with no initial stresses or strains, the deformation energy of an elastic body submitted to externally applied forces can be expressed as [13]:

$$E = \frac{1}{2}\int_{\Omega} \sigma^T \epsilon \, d\Omega + \int_{\Omega} \boldsymbol{F}^T \boldsymbol{u} \, d\Omega, \tag{1}$$

where $\boldsymbol{u} = \boldsymbol{u}(\boldsymbol{x})$ is the displacement vector, $\boldsymbol{F} = \boldsymbol{F}(\boldsymbol{x})$ the vector representing the forces applied to the elastic body (forces per unit volume, surface forces or forces concentrated at nodes), and Ω the body on which one is working.

In the case of linear elasticity, each stress component (σ) is directly proportional to each strain component (ϵ), linked by the elastic stiffnesses, D_{ijkl} which compose a fourth-rank tensor and reduce to a 6x6 symmetric matrix for a general anisotropic material.

In the case of an orthotropic material, the material has three mutually perpendicular planes of elastic symmetry. Hence there are three kinds of material parameters necessary to compute the stiffness matrix: 1) the Young's moduli E_i relate tension and the stretch in the main orthogonal directions, 2) the shear moduli G_{ij} relate tension and stretch in other directions than those of the planes of elastic symmetry, and 3) the Poisson's ratios ν_{ij} represent the ratio of the lateral contraction due to longitudinal stress in a given plane. The determination of these parameters and the assembly of the stiffness matrix are explained in Section 2.3.

2.2 FEM Framework

Within a finite element discretization framework, an elastic body is approximated as an assembly of discrete finite elements interconnected at nodal points on the element boundaries. The continuous displacement field $\mathbf{u}$ within each element is approximated as a function of the displacement at the element's nodal points $\mathbf{u}_i^{el}$ weighted by its shape functions $N_i^{el} = N_i^{el}(\mathbf{x})$. Through such a discretization, and because the integral over the whole domain can be seen as the sum of the integrals over every element, it is possible to evaluate the equilibrium equations separately on every element, and to sum up the contribution of every element to which a vertex is connected to build a global equilibrium matrix system.

For every node i of each element el, we define the matrix $\mathbf{B}_i^{el} = \mathbf{L}_i N_i^{el}$. Using that definition and then minimizing the energy in Equation 1 with respect to the displacement of each element, we have:

$$\int_\Omega \sum_{j=1}^{N_{nodes}} \mathbf{B}_i^{el^T} \mathbf{D} \mathbf{B}_j^{el} \mathbf{u}_j^{el} \, d\Omega = -\int_\Omega \mathbf{F} N_i^{el} \, d\Omega \quad ; \qquad i = 1, \cdots, N_{nodes} \tag{2}$$

This expression can be written as a matrix system for each finite element, and the assembly of the local matrices then leads to a global system

$$\mathbf{K}\mathbf{u} = -\mathbf{F}, \tag{3}$$

the solution of which will provide us with the deformation field corresponding to the global minimum of the total deformation energy. Given externally applied forces $\mathbf{F}$ to a discretized body characterized by a rigidity matrix $\mathbf{K}$, solving the previous equation provides us with the resulting displacements.

2.3 Diffusion Tensor MRI

DT-MRI is a technique developed to allow non-invasive quantification of diffusion of water *in vivo*. The directional dependence of water diffusion rates can be closely related to the anisotropy of the structure. Therefore, DT-MRI can be used to infer the organization of tissue components.

In the brain, high anisotropy reflects both the underlying highly directional arrangement of white matter fiber bundles forming white matter tracts and their intrinsic microstructure. This anisotropy can be characterized to distinguish the principal orientation of diffusion, corresponding to the dominant axis of the bundles of axons making up white matter tracts in an given voxel. Because different histologic types of brain white matter demonstrate significant and reproducible anisotropy differences [9], it would be expected that they would deform differently and thus should be modeled differently.

To incorporate the white matter structure into the biomechanical model, the local coordinate system aligned with the fiber direction and its corresponding elasticity parameters must be defined for the stiffness matrix calculation at each tetrahedron. Diagonalization of the corresponding symmetric 3x3 diffusion tensor gives three pairs of eigenvalues and mutually orthogonal eigenvectors. Since molecular diffusion is hindered by encounters with cell membranes and cytoskeletal structures, the water diffusion rate parallel to a fiber is higher than perpendicular to it. The principal eigenvector is therefore parallel to the local tangent of a fiber.

The stiffness matrix for a transversely isotropic material requires 5 independent parameters. Cross-fiber stiffness is approximately 2x to 10x greater than the fiber stiffness for anisotropic brain tissue [8]. We have only limited confidence in using these results for our model because the measurements of fiber stiffnesses are in very specific regions of the brain, such as the corpus callosum and corona radiata, and the stiffness ratios differ throughout. There is currently no measure of how the stiffness ratio relates to anisotropy of diffusion. As an initial attempt to relate the results of DT-MRI and material properties of the brain tissue, we calculate fractional anisotropy (FA) from the eigenvalues of the diffusion tensor and the Young's modulus in the cross-fiber direction p as a linear function of the FA, maximum stiffness ratio (α), and the Young's modulus in the fiber direction f.

$$E_p = (1 + (\alpha - 1)FA)E_f \qquad E_f = E \tag{4}$$

The Poisson's ratios are assumed to be equal in all three directions because the compressibility of the tissue is not expected to change. The shear moduli are calculated from the Young's moduli and Poisson's ratios as follows:

$$G_f = G_p = \frac{E_p}{2(1+\nu)} \tag{5}$$

G_f is actually an independent parameter, but it is arbitrarily set equal to the shear modulus in the plane of isotropy because the experiments for the elasticity parameters for anisotropic brain tissue focus do not include the shear moduli.

Once the local stiffness matrix has been determined, it is rotated according to the transformation matrix to the global coordinate system from the local coordinate system, as defined by the eigenvectors.

2.4 Non-rigid Registration Algorithm

The steps of the registration method are summarized as follows: **Preoperative image acquisition, processing and visualization**: Before the surgery, a conventional grey-scale MRI scan, functional MRI, MRA, and DT-MRI datasets are acquired. These images are processed to locate the ventricles, cortical surface, tumor, white matter tracts, and blood vessels, and are manually registered to the grey-scale MRI. 3D Slicer [3], an integrated software tool, is used for visualization and surgical planning. **Intraoperative image acquisition**: The open configuration 0.5 T MR scanner is used to acquire intraoperative scans as necessary. **Intraoperative rigid registration**: The presurgical data is registered to the intraoperative scan using an automated, Mutual Information-based algorithm [11], and is resampled to correspond to the dimensions of the intraoperative data, a 256x256x60 matrix with voxels 0.859375x0.859375x2.5 mm^3. **Intraoperative non-rigid registration**: An active surface matching algorithm deforms the preoperative surface meshes of the brain and ventricles to the corresponding segmentations of the intraoperative target. The resulting surface displacements serve as boundary conditions to the biomechanical model, which solves for the volumetric deformation. Preoperative models and grey-scale image data are deformed according to the resulting displacement field. **Intraoperative visualization**: The combined data is visualized using 3D Slicer, which includes the optical tracking system (Figure 1). Further details on processing and data acquisition parameters are available in [5].

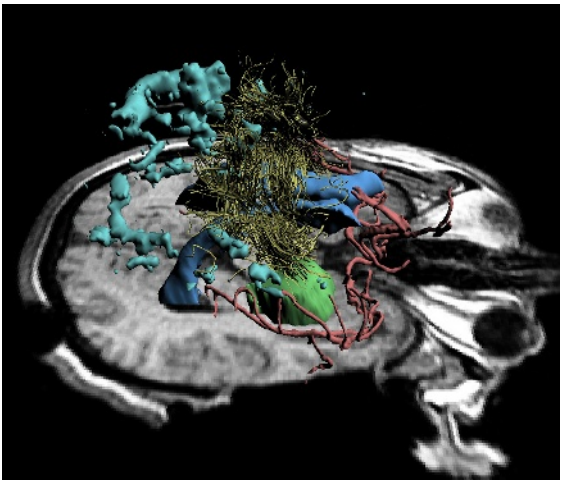

Fig. 1. Preoperative models (white matter tracts are shown in yellow, blood vessels in red, tumor in green, ventricles in blue, and fMRI activation in aqua) deformed according to the FEM calculations and superimposed on an intraoperative axial slice.

3 Registration Results

For the three surgical cases in which DT-MRI data was acquired, the volumetric deformation was applied using both the isotropic and anisotropic linear elastic models given the same initial surface displacement boundary conditions. The default values for the Young's modulus were defined consistently with the previous work ($E = 3000Pa$ for the brain and $E = 1000Pa$ for the ventricles) on the isotropic FEM [2]. Poisson's ratio was set to be 0.35 because that was the closest setting to the previous value of 0.45 that would yield a solution that satified the boundary conditions. The optimal maximum stiffness ratio (α) is 10 using these parameters.

Landmark Displacement Error. Accuracy was evaluated given a set of landmarks indentified by a neurosurgeon in both the preoperative and intraoperative image for one surgical case. These landmarks include the medial tumor margin, 3 points on the lateral temporal lobe surface, and the optic tract. We compared the registration errors of both the isotropic and anisotropic models, as well as the original rigid registration (Table 1). These displacement errors are all very

Table 1. Comparison of error in landmark displacement for rigid registration, the isotropic model, and the isotropic model for one surgical case.

Landmark Location	Rigid Reg.	Isotropic	Anisotropic
Medial Tumor Margin	1.000 mm	0.357 mm	0.357 mm
Lateral Temporal Lobe Surface (1)	7.211 mm	7.343 mm	7.143 mm
Lateral Temporal Lobe Surface (2)	2.236 mm	1.510 mm	1.512 mm
Lateral Temporal Lobe Surface (3)	2.236 mm	2.584 mm	2.559 mm
Optic Tract	2.236 mm	2.236 mm	2.236 mm
Average Error	2.984 mm	2.806 mm	2.761 mm

similar, and there is a limited number of landmarks, but it appears that the anisotropic model does show a minimal amount of improvement. However, to better characterize how the isotropic and anisotropic models differ throughout the volume, we consider the entire deformation fields in the next section.

Deformation Fields. For a quantitative analysis of the differences in the deformation fields, Table 2 shows the maximum displacement difference in each of the three axes, the maximum displacement difference, the mean displacement difference, and the percentage of the maximum displacement. There is a substantial difference in the deformations relative to the displacement when anisotropy is included in the model. The greatest differences in the deformation fields tend to occur in regions of high anisotropy. Though this does not directly show an improvement in accuracy, it does show that including anisotropy does change the registration result.

Table 2. Differences in deformation fields between the anisotropic and isotropic models, over each of the three surgical cases.

	dx_{max}	dy_{max}	dz_{max}	D_{max}	D_{mean}	$D_{\%}$
Case 1	1.06 mm	1.30 mm	2.60 mm	2.92 mm	0.174 mm	22.6%
Case 2	0.36 mm	0.56 mm	1.14 mm	1.14 mm	0.141 mm	10.7%
Case 3	0.51 mm	0.54 mm	2.08 mm	2.08 mm	0.152 mm	24.5%

3.1 Computation Time Analysis

The time constraints of a neurosurgical procedure require consideration of the additional computation time required to assemble and solve the more complex model. For the purpose of this experiment, we focus only on the assembly and solution time because the additional time required (approximately 9 minutes) for segmentation, rigid registration, applying deformation fields, etc. are unchanged from [10].

Two major factors determine the time required for the Finite Element model. The first is the size and connectivity of the mesh (see [2] for meshing details), which affects both the isotropic and anisotropic computation times. The second is the amount of DT-MRI data available for the mesh. Table 3 shows that in general, the anisotropic model requires about twice as long as the isotropic one to be assembled and solved. However, this only increases the total time required, including pre-processing, assembling and solving the FEM, and revisualizing the data in Slicer, from 12 minutes to 14 minutes, which is still very reasonable, especially considering the rapid increases in computational power.

Table 3. Computation time comparison between anisotropic and isotropic models.

	Isotropic Model	Anisotropic Model	DTI Dataset Size
Case 1	65.6 sec	118.1 sec	256x256x6
Case 2	87.7 sec	175.1 sec	256x256x18
Case 3	97.9 sec	188.3 sec	256x256x19

4 Discussion and Conclusion

We demonstrated that that a biomechanical model of anisotropic white matter elasticity enabled improved localization of white matter tracts during surgical resection. We used a set of landmarks identified by a neurosurgeon to evaluate the relative accuracy of the new model, which showed slight improvement with the anisotropic model. To account for displacement differences that occurred where there were no landmarks identified, we compared the deformation fields directly.

The differences in displacement was between 1 and 3 mm for each surgical case, which is up to nearly 25% of the total maximum displacement due to brain shift. For future surgical cases with greater amounts of brain shift, we expect that the improvement in registration accuracy will be more substantial. Finally, we showed that the computation time required for the anisotropic model was approximately twice that of that of the isotropic model, but still on the order of about three minutes, adequate for near real-time use.

Acknowledgements. This investigation was supported by a research grant from the Whitaker Foundation, by NIH grants R21 MH67054, R01 LM007861, P41 RR13218 and P01 CA67165, and by the NSF ERC grant (JHU Agreement #8810-274).

References

1. C. Davatzikos. Spatial transformation and registration of brain images using elastically deformable models. *Computer Vision and Image Understanding*, 66(2):207–222, 1997.
2. M. Ferrant. *Physics-based deformable modeling of volumes and surfaces for medical image registration, segmentation and visualization.* PhD thesis, Université Catholique de Louvain, April 2001.
3. D. T. Gering, A. Nabavi, R. Kikinis, N.. Hata, L. J. O'Donnell, W. E. Grimson, F. A. Jolesz, P. McL. Black, and W. M. Wells III. An integrated visualization system for surgical planning and guidance using image fusion and an open mr. *Journal of Magnetic Resonance Imaging*, 13:967–975, 2001.
4. A. Hagemann, K. Rohr, H. S. Stiehl, U. Spetzger, and J. M. Gilsbach. Biomechanical modeling of the human head for physically based, nonrigid image registration. *IEEE Transactions on Medical Imaging*, 18(10):875–884, October 1999.
5. C. A. Kemper. Incorporation of diffusion tensor mri in non-rigid registration for image-guided neurosurgery. Master's thesis, Massachusetts Institute of Technology, June 2003.
6. M. I. Miga, K. D. Paulsen, J. M. Lemery, S. D. Eisner, A. Hartov, F. E. Kennedy, and D. W. Roberts. Model-updated image guidance: Initial clinical experiences with gravity-induced brain deformation. *IEEE Transactions on Medical Imaging*, 18(10):866–874, October 1999.
7. K. Miller and K. Chinzei. Mechanical properties of brain tissue in tension. *Journal of Biomechanics*, 35:483–490, 2002.
8. M. T. Prange and S. S. Margulies. Regional, directional, and age-dependent properties of the brain undergoing large deformation. *Transactions of the ASME*, 124:244–252, April 2002.
9. J. S. Shimony, R. C. McKinstry, E. Akbudak, J. A. Aronovitz, A. Z. Snyder, N. F. Lori, T. S. Cull, and T. E. Conturo. Quantitative diffusion tensor anisotropy brain mr imaging: normative human data and anatomic analysis. *Radiology*, 212:770–784, 1999.
10. A. Tei. Multi-modality image fusion by real-time tracking of volumetric brain deformation during image guided neurosurgery. Master's thesis, Massachusetts Institute of Technology, February 2002.

11. W. M. Wells, P. Viola, H. Atsumi, S. Nakajima, and R. Kikinis. Multi-modal volume registration by maximization of mutual information. *Medical Image Analysis*, pages 35–51, March 1996.
12. J. D. West, K. D. Paulsen, S. Inati, F. Kennedy, A. Hartov, and D. W. Roberts. Incorporation of diffusion tensor anisotropy in brain deformation models for updating preoperative images to improve image-guidance. In *International Symposium on Biomedical Imaging*, pages 509–512, 2002.
13. O. C. Zienkewickz and R. L. Taylor. *The Finite Element Method*, volume 1. McGraw-Hill Book Company, 4 edition, 1987.